Available online at www.sciencedirect.com
SCIENCE DIRECT®
Journal of Solid State Chemistry 175 (2003) 52–58
JOURNAL OF SOLID STATE CHEMISTRY
http://elsevier.com/locate/jssc

Effects of vacancy concentration on the magnetic and transport properties of $(La_{1-x}Pb_x)_{1-y}\square_yMnO_3$

Guerman Popov, Jacob Goldsmith, and Martha Greenblatt*

Department of Chemistry and Chemical Biology, Rutgers, The State University of New Jersey, 610 Taylor Road, Piscataway, NJ 08854-8087, USA

Received 6 January 2003; received in revised form 10 February 2003; accepted 16 February 2003

Abstract

$(La_{1-x}Pb_x)_{1-y}\square_yMnO_3$ with $x = 0.05-0.5$ and $y = 0$, 0.05, 0.1 (where $\square$ is a vacancy) was studied to evaluate the effects of *A*-site vacancies on the physical properties. In this system manganese perovskites form with tolerance factors close to 1 and low *A*-site cation size mismatch due to similarities in the effective ionic radii of La^{3+} and Pb^{2+}. Increasing vacancy concentration indicates no significant effect on the lattice parameters or volume. However, the vacancies introduce a greater *A*-site cation size mismatch, which leads to a lowering of the ferromagnetic and metal–insulator transition temperatures, although the transitions are not broadened with increasing vacancy content. Due to the vacancies a distribution of Mn–O–Mn angles and Mn–O distances are created, and long range order in $(La_{1-x}Pb_x)_{1-y}\square_yMnO_3$ appears to be determined by Mn–O–Mn angles and Mn–O distances which most distort from 180° and are the longest, respectively, in the structure.

1. Introduction

Perovskite materials of general composition ABO_3 exhibit many interesting properties with important technological applications. Some of the important properties include, but are not limited to, colossal magnetoresistance (CMR), superconductivity, charge ordering, ferroelectricity, and high dielectric constant. A three-dimensional (3D) network of interconnecting octahedra BO_6 can provide optimal metal–oxygen–metal angles and distances for orbital mixing that can lead to diverse effects. While in the ideal cubic structure the metal–oxygen–metal angles are 180°, the perovskite structure can distort to various degrees depending on the sizes and nature of the constituent ions.

In a typical CMR material the ferromagnetic ordering is accompanied by an insulator–metal transition. Rodriguez-Martinez and Attfield [1] showed that the optimal *A*-site average cation size that results in a tolerance factor close to 1 in $Ln_{0.7}M_{0.3}MnO_3$ manganites produces a material with the highest Curie temperature, T_c. The tolerance factor (t) is a quantitative measure of the structural perfection of the ABO_3 perovskites:

$$t = \frac{r_A + r_O}{\sqrt{2}(r_A + r_O)},$$

where r_A is the ionic radius of 12-coordinated *A* cation, r_B is the ionic radius of 6-coordinated *B* cation, and r_O is the ionic radius of oxygen. The closer the tolerance factor is to unity, the closer is the structure to the "ideal" cubic perovskite and the closer are the *B*–O–*B* bond angles to 180°.

The average ionic radius of the *A*-site can be varied by the presence of different rare earths and divalent cations. However, different ions on the *A*-site lead to disorder, because of size mismatch, and suppression of T_c [1]. The disorder can be quantitatively expressed by the variance factor, $\sigma^2 = \langle r_A^2 \rangle - \langle r_A \rangle^2$, where $\langle r_A \rangle$ is the average *A*-site cation radius [1]. Since there are no 3+ and 2+ cations whose effective ionic radii are identical, or close to each other, *A*-site disorder will always exist in $Ln_{1-x}M_xMnO_3$ perovskite manganites. Therefore, the hypothetical highest possible T_c can never be achieved. Attfield [2] studied the effect of σ^2 on the properties of several perovskite systems where the *A*-site disorder was induced by cations of different sizes; however, there has been no investigation on how the vacancies affect σ^2 and the properties.

*Corresponding author. Fax: 732-445-5312.
E-mail address: greenblatt@rutchem.rutgers.edu (M. Greenblatt).

0022-4596/03/$ - see front matter © 2003 Elsevier Science (USA). All rights reserved.
doi:10.1016/S0022-4596(03)00135-X

Using the published ionic radii [3] the "ideal" average effective *A*-site cation radius, $\langle r_A \rangle$ for the perovskite manganite $Ln^{3+}_{0.7}M^{2+}_{0.3}Mn^{3+}_{0.7}Mn^{4+}_{0.3}O_3$ is 1.443 Å. Trivalent and divalent cations suitable for perovskite *A*-site with effective ionic radii close to the "ideal" are: Ca^{2+} (1.34 Å), La^{3+} (1.36 Å), Sr^{2+} (1.44 Å), Pb^{2+} (1.49 Å), and Ba^{2+} (1.61 Å). There must be a mixture of 3+ and 2+ cations on the *A*-site. While the ionic radius of Sr^{2+} (1.44 Å) is closer to that of La^{3+} (1.36 Å) and is a very good match to the "ideal" average *A*-site ionic radius (1.443 Å), the average radius that results from the mixture of La^{3+} and Sr^{2+} will always be lower than 1.443 Å. The next suitable 2+ cation with higher radius is Pb^{2+}. A mixture of La^{3+} and Pb^{2+} on the *A*-site could produce an average radius suitable for a perovskite manganite with t closest to 1. Moreover, La^{3+} and Pb^{2+} whose radii are relatively close to each other and to $\langle r_A \rangle = 1.443$ Å will produce a minimal variance factor σ^2 in comparison with, for example, La^{3+} and Ba^{2+}.

It is known that vacancies on the *A*-site of perovskite serve as hole dopants increasing the oxidation state of Mn. At low-level, vacancies usually increase T_c. For example, ferromagnetic $La_{1-x}\square_xMnO_3$ compositions with relatively high T_c were obtained [6]; $La_{0.83}Sr_{0.13}\square_{0.04}MnO_{2.98}$ was found to have $T_c = 334$ K, which is higher than expected for this level of Sr substitution [4]. For $Pr_{0.7-x}\square_xSr_{0.3}MnO_3$ T_c increases with increasing x [5]. However, the influence of vacancies on the variance factor σ^2, where the effective "radius of a vacancy" is not easily determined, and the expected consequent changes in T_c have not been studied.

The $(La_{1-x}Pb_x)_{1-y}\square_yMnO_3$ system forms perovskites with $t \sim 1$ and small values of σ^2 for mixed La^{3+} and Pb^{2+} and thus allows the study of the affect of vacancies on the physical properties without the influence of other factors (i.e., *A*-site cation mismatch, large distortion from cubic symmetry or poor *B*–O–*B* overlap).

In 1950, Jonker and Van Santen [7] first reported on the highly conducting ferromagnetic $La_{0.7}Pb_{0.3}MnO_3$ and $La_{0.6}Pb_{0.4}MnO_3$ systems with T_c's of 361 and 337 K, respectively. In 1994 Manoharan et al. [8] reported high magnetoresistance (MR) (40%) at 300 K and 6 T in $La_{0.6}Pb_{0.4}MnO_3$ thin film. In 1995, Mahendiran et al. [9] showed that all the compositions in the range of $0.1 \leqslant x \leqslant 0.5$ for $La_{1-x}Pb_xMnO_3$ exhibited a peak in the MR at ~300–340 K. Although the $La_{1-x}Pb_xMnO_3$ system has been well studied, $(La_{1-x}Pb_x)_{1-y}\square_yMnO_3$ has not been investigated systematically before.

In this paper, we present a systematic study of $(La_{1-x}Pb_x)_{1-y}\square_yMnO_3$ with $x = 0.05-0.5$ and $y = 0$, 0.05, 0.1. Magnetization, resistivity, and MR results are evaluated in terms of the unit-cell parameters and the manganese oxidation states.

2. Experimental

All the samples were synthesized by the Pechini technique [10] under the same conditions. Stoichiometric amounts of La_2O_3 (Alfa 99.9%, annealed at 1000°C overnight), PbO (Fisher, certified, dried at 150°C overnight) were dissolved in dilute (10%) HNO_3, and a stoichiometric amount of 49.7% $Mn(NO_3)_2$ solution (Aldrich) was added. Then appropriate amounts of citric acid and ethylene glycol were added and the solution was slowly evaporated. The gels were dried at 300°C, and fired at 600°C in air to remove the organic matter, and to decompose the nitrates. The products were pressed into pellets and sintered at 700°C for 10 h, then heated to 1000°C and sintered for 13 h. The samples were then quenched in air by removal from the furnace.

Powder X-ray diffraction (PXD) data were obtained with a Scintag PAD V and a Bruker Advance D8 diffractometer (Cu$K\alpha$ radiation) in the range of 10–80° 2θ. The PXD patterns were analyzed by profile matching (Le Bail) with the TOPAS program [11] using the fundamental parameters approach. Magnetic measurements were performed with a Quantum Design SQUID magnetometer (MPMS-*XL*). MR and resistivity measurements were made on the same MPMS-*XL* with External Device Control and Keithley equipment by standard four-probe technique. Gold wire contacts were attached to the sample with silver paint. MR was measured as follows: the resistivity was measured at a given temperature without an applied magnetic field, then the magnetic field was turned on and the resistivity was measured; the field was turned off, and the temperature was changed to the next value. This procedure was repeated for the entire range of temperatures measured. The measurement of MR in this way is closest to the conditions for real applications of magnetoresistive materials, and ensures that the sample is in the same state for the measurement of resistivity in different fields.

3. Results and discussion

3.1. Structural characterization

The Pechini synthesis technique was chosen to minimize possible Pb evaporation from the system due to the low melting point (790°C) and high vapor pressure of PbO. PXD on selected samples show that the majority phase formed after gel decomposition at 600°C is perovskite, although with poor crystallinity. After annealing the samples at higher temperatures as described in the "Experimental" section the crystallinity improved. Chemical analysis by ICP on selected samples showed that the lead content of the samples is within 4% of the target. This precision is acceptable, since the

properties of the samples will be compared with each other. Also the oxygen content should be very similar throughout the series, because all the samples were synthesized at the same conditions. Quenching of the samples was carried out to prevent pick-up of excess oxygen.

$(La_{1-x}Pb_x)_{1-y}\square_yMnO_3$ compositions with $x = 0.05$, 0.1, 0.2, 0.3, 0.4, 0.5 and $y = 0$, 0.05, 0.1 formed as single phases (Fig. 1). Samples with $x = 0.6$ synthesized at these conditions showed $Pb_3Mn_6O_{13}$ as an impurity, which was consistent with the solubility limit of Pb. While the solubility limit can probably be increased by changing the synthesis conditions, it is not the goal of this study, and identical conditions of synthesis are required for comparison of the samples studied.

All the compositions obtained crystallize in rhombohedral symmetry, and $R\bar{3}c$ space group in hexagonal setting was used for the profile matching. In Fig. 1, the PXD patterns for samples with $y = 0$ show that with increasing Pb content the distortion from cubic symmetry is decreasing; this can be expressed quantitatively by the lattice parameter relationships. For cubic perovskites: $a_{hex} = a_c\sqrt{2}$ and $c_{hex} = a_c2\sqrt{3}$, where a_{hex}, c_{hex} are the lattice parameters in hexagonal setting, and a_c is that in cubic setting. For a distorted (from cubic symmetry) perovskite $q = (c_{hex}/2\sqrt{3})/(a_{hex}/\sqrt{2})$ will approach 1 as the symmetry approaches cubic. Fig. 2 shows a 3D plot of q vs. x and y for $(La_{1-x}Pb_x)_{1-y}\square_yMnO_3$. The q parameter approaches 1 as the Pb content increases but never reaches it (error bars are smaller than the data points shown).

Since there are two variable lattice parameters in rhombohedral symmetry, it is convenient to compare unit cell volumes. Fig. 3 represents a 3D plot of unit-cell volumes for the studied compositions. Since the ionic

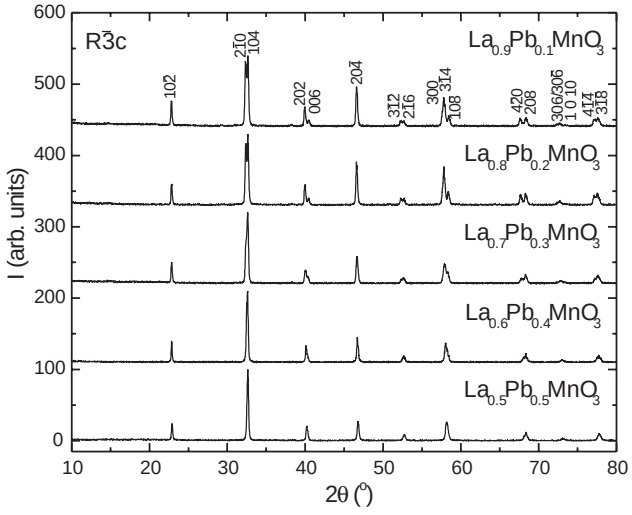

Fig. 1. X-ray diffraction patterns of the $(La_{1-x}Pb_x)_{1-y}\square_yMnO_3$ samples with $y = 0$. Indexing is in hexagonal setting.

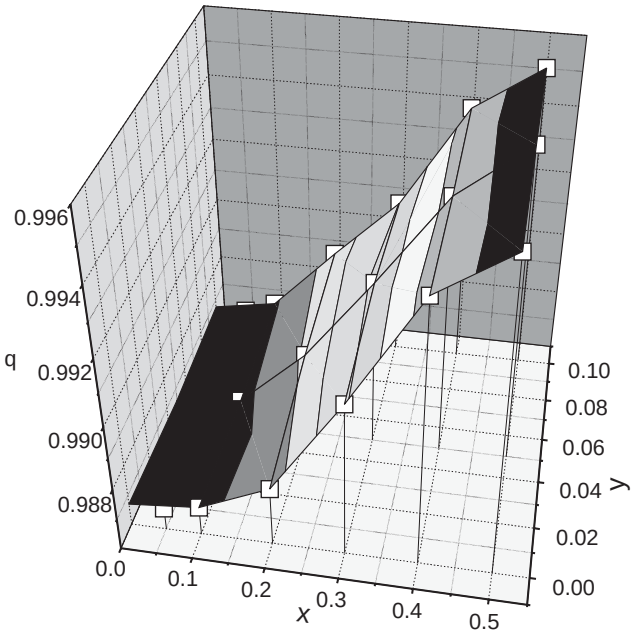

Fig. 2. 3D plot of q vs. x and y in $(La_{1-x}Pb_x)_{1-y}\square_yMnO_3$, where $q = (c_{hex}/2\sqrt{3})/(a_{hex}/\sqrt{2})$; a_{hex} and c_{hex} are lattice parameters.

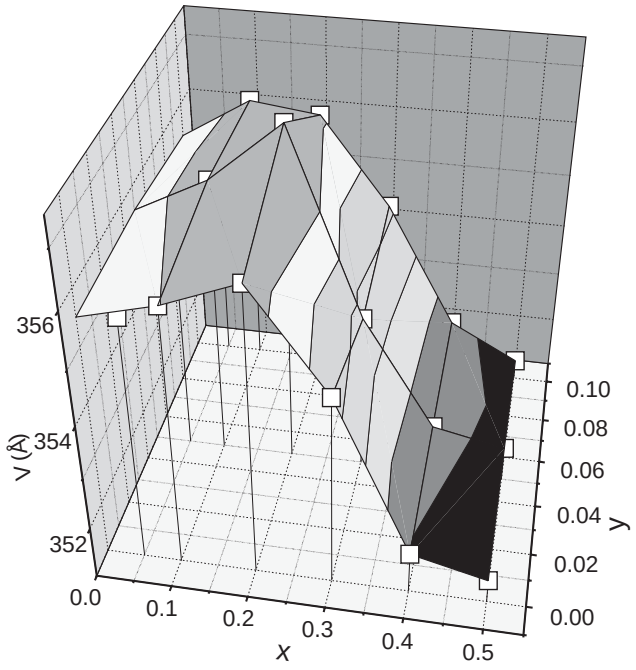

Fig. 3. 3D plot of unit-cell volume vs. x and y in $(La_{1-x}Pb_x)_{1-y}\square_yMnO_3$.

radius of Pb^{2+} is larger than that of La^{3+}, the unit-cell volume (V) first increases with increasing Pb content up to $x = 0.2$; with further increase of Pb concentration the V decreases, because Mn^{4+} (0.53 Å) is smaller than Mn^{3+} (0.645 Å) and $Mn^{3+/4+}$ located at the center of MnO_6 octahedra, the building frame of perovskite,

affect the volume more critically. Furthermore, a higher Pb content corresponds to a lower Jahn–Teller Mn^{3+} content with distorted oxygen environment. Thus a lower content of distorted Mn^{3+} (and more Mn^{4+}) would even further decrease the unit-cell volume, which explains the steep decrease seen for $x = 0.2-0.5$ (Fig. 3). The same argument applies to Fig. 2 for the steep increase of the q parameter for $x = 0.2-0.5$. However, the presence of Jahn–Teller distorted Mn^{3+} in $(La_{1-x}Pb_x)_{1-y}\square_yMnO_3$ even at high Pb content cannot allow the distortions to vanish completely, thus the q parameter never reaches 1, and the structure is distorted from ideal cubic symmetry.

Another observation noted from the analysis of Figs. 2 and 3 is that with increasing vacancy levels (y in $(La_{1-x}Pb_x)_{1-y}\square_yMnO_3$) the unit-cell volume and the q parameter do not change significantly. This is not surprising, as vacancies on the A-site of perovskites do not lead to a collapse of the structure as exemplified by ReO_3. Nevertheless, the effective "radius of a vacancy" must affect the variance factor, σ^2 and concomitantly the properties, as shown below.

3.2. Magnetic and transport properties

Since the magnetic and transport properties of $(La_{1-x}Pb_x)_{1-y}\square_yMnO_3$ depend on the average manganese oxidation state, samples with approximately the same Mn oxidation state are compared in the evaluations. Table 1 provides the calculated oxidation states of manganese based on the starting compositions of the samples with various x and y. Fig. 4 shows the magnetic

Table 1
Average manganese oxidation states in $(La_{1-x}Pb_x)_{1-y}\square_yMnO_3$ calculated based on starting composition

x	y		
	0	0.05	0.1
0.05	3.05	3.1975	3.345
0.1	3.1	3.245	3.39
0.2	3.2	3.34	3.48
0.3	3.3	3.435	3.57
0.4	3.4	3.53	3.66
0.5	3.5	3.625	3.75

$(La_{1-x}Pb_x)_{1-y}\square_yMnO_3$

xly	0	0.05	0.1
0.05	3.05	3.1975	**3.345**
0.1	3.1	3.245	3.39
0.2	3.2	**3.34**	3.48
0.3	**3.3**	3.435	3.57
0.4	3.4	3.53	3.66
0.5	3.5	3.625	3.75

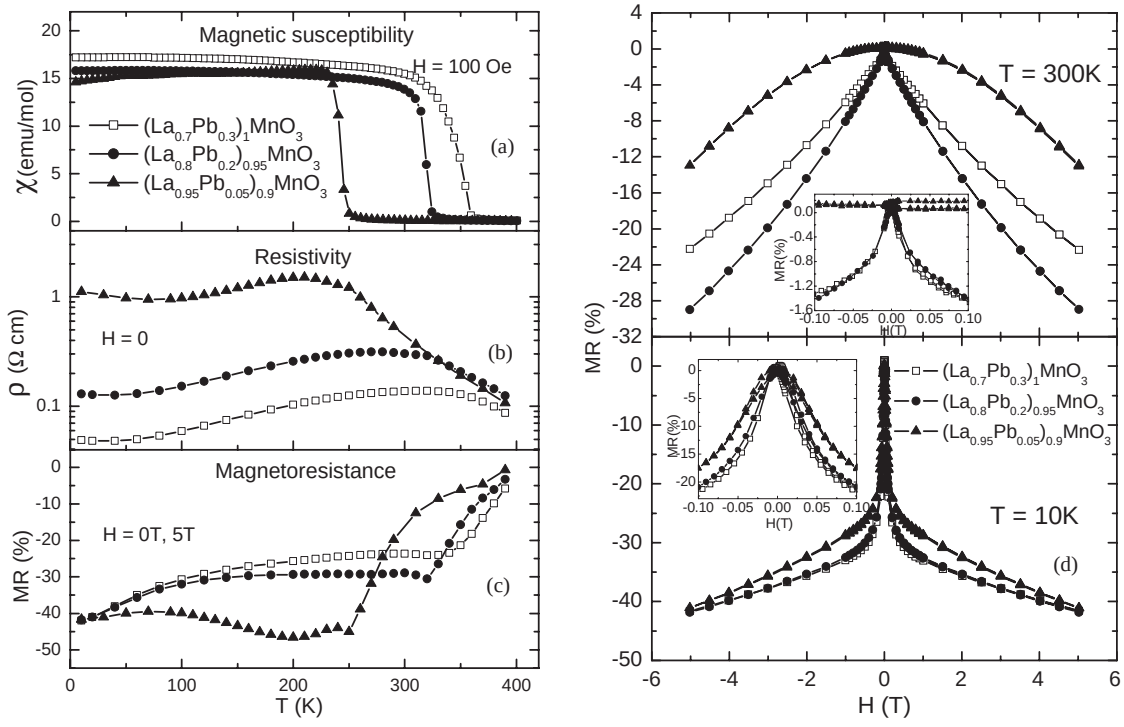

Fig. 4. Temperature-dependent magnetic susceptibility, χ (a), resistivity, ρ (b), MR (c), and field-dependent MR (d) of the samples highlighted in the table.

$(La_{1-x}Pb_x)_{1-y}\square_yMnO_3$

x\y	0	0.05	0.1
0.05	3.05	3.1975	3.345
0.1	3.1	3.245	**3.39**
0.2	3.2	3.34	3.48
0.3	3.3	**3.435**	3.57
0.4	**3.4**	3.53	3.66
0.5	3.5	3.625	3.75

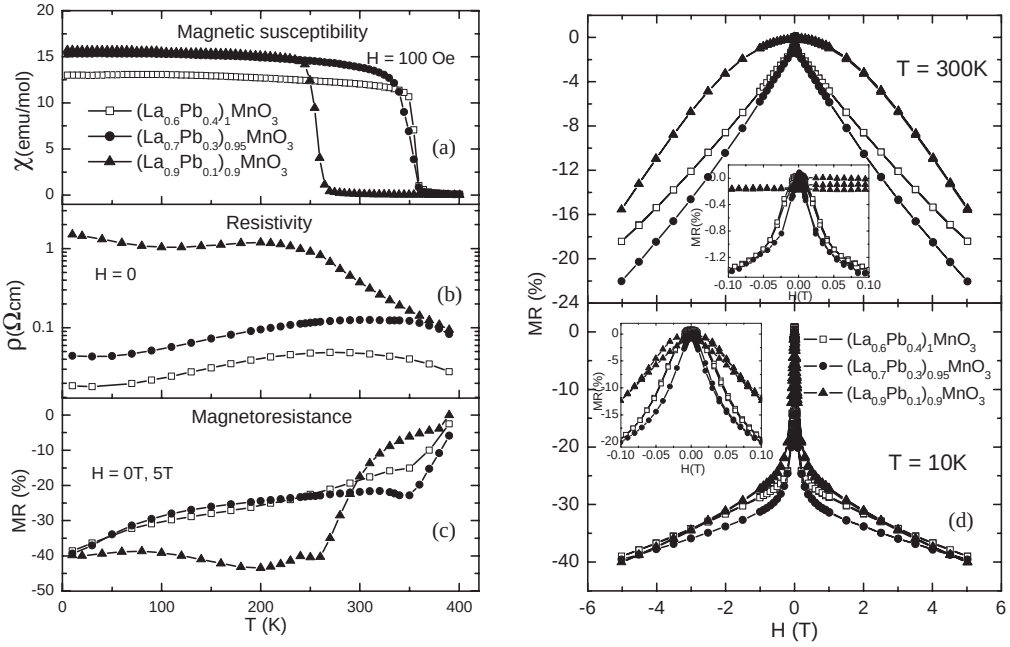

Fig. 5. Temperature-dependent magnetic susceptibility χ (a), resistivity, ρ, (b), MR (c), and field-dependent MR (d) of the samples highlighted in the table.

and transport data for three samples with the average manganese oxidation state $\sim +3.3$. In Figs. 5 and 6 the data are presented for samples with $Mn^{3.4+}$ and $Mn^{3.5+}$, respectively.

The temperature dependence of the magnetic susceptibility, χ, in Fig. 4a shows that while the average Mn oxidation states are nearly identical, T_c is the lowest for the sample with the highest vacancy concentration, and the highest for that with the lowest vacancy concentration. The same trend can be seen for the series with $Mn^{3.4+}$ and $Mn^{3.5+}$ (Figs. 5a and 6a), while the T_c's of the samples are higher within these latter series as expected. In addition, the samples with $y = 0.1$ have significantly lower T_c's compared to the samples with $y = 0.05$ and 0 in $(La_{1-x}Pb_x)_{1-y}\square_yMnO_3$ whose T_c's are close to each other, suggesting that only a significant amount of vacancies affects the T_c considerably. Metal–insulator transitions near the T_c's are observed for all the samples in the temperature dependent resistivity (Figs. 4b, 5b and 6b). The samples with higher vacancy concentration have higher resistivity in the temperature range measured.

The absolute value of the temperature-dependent MR of all the samples has a maximum around T_c's (Figs. 4c, 5c and 6c), which is attributed to intra-grain MR. At low temperatures the MR increases again to about 40%; in this region inter-grain spin polarized tunneling MR appears to dominate [12]. A trend resembling the dependence of T_c's on vacancy concentration is observed for the low-temperature (10 K) field-dependent MR (Figs. 4d and 5d, magnified in insets). The lowest low-field MR (absolute value) is observed for samples with the highest vacancy concentrations (y). Such a comparison of the samples with $Mn^{3.5+}$ (Fig. 6d) does not allow any definitive conclusion, because their low-field MR–H curves are within experimental error.

The behavior described above may be attributed to the presence of vacancies, which lead to a distribution of Mn–O–Mn angles and Mn–O distances within the perovskite structure. Mn–O–Mn angles close to 180° (ideal cubic perovskite) lead to enhanced magnetic (higher T_c) and transport properties [1]. While on average the Mn–O–Mn angles may be close to 180° in $(La_{1-x}Pb_x)_{1-y}\square_yMnO_3$, in the vacancy-rich samples ($y = 0.1$) the random distribution of vacancies creates regions where the Mn–O–Mn bond angles deviate significantly from 180°. The presence of such regions would be expected to induce a broadening of the ferromagnetic transitions; however, the transitions observed in this study are quite sharp (Figs. 4a, 5a and

$(La_{1-x}Pb_x)_{1-y}\square_yMnO_3$

x\y	0	0.05	0.1
0.05	3.05	3.1975	3.345
0.1	3.1	3.245	3.39
0.2	3.2	3.34	**3.48**
0.3	3.3	3.435	3.57
0.4	3.4	**3.53**	3.66
0.5	**3.5**	3.625	3.75

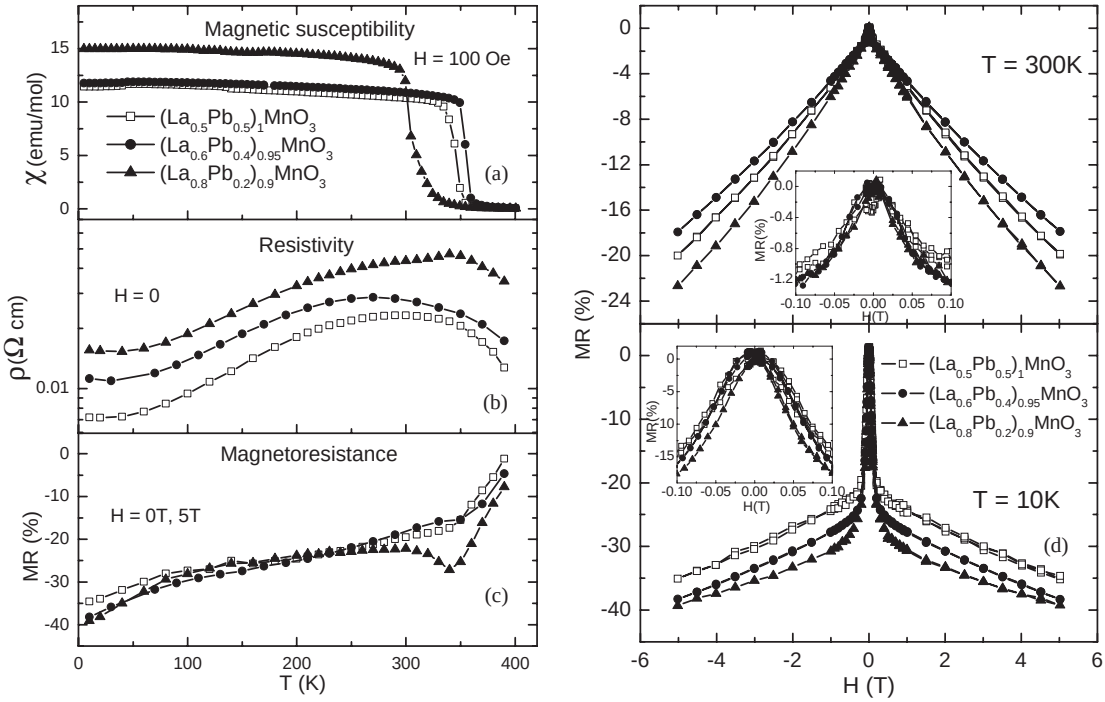

Fig. 6. Temperature-dependent magnetic susceptibility, χ (a), resistivity, ρ (b), MR (c), and field-dependent MR (d) of the samples highlighted in the table.

6a). Nonetheless, the T_c's of vacancy-rich samples are lower. This leads to the conclusion that the long range order in $(La_{1-x}Pb_x)_{1-y}\square_yMnO_3$ is determined by the Mn–O–Mn angles most distorted from the ideal 180° and the Mn–O distances that are longest within the distribution. This conclusion is inline with the results of Rodriguez-Martinez and Attfield [1], which show that increasing A-site cation size mismatch (σ^2) decreases T_c and the metal–insulator transition temperature in perovskite manganites. In $(La_{1-x}Pb_x)_{1-y}\square_yMnO_3$ the cation size mismatch is induced by vacancies.

4. Conclusions

The effect of A-site vacancy concentration on the magnetic and transport properties of the $(La_{1-x}Pb_x)_{1-y}\square_yMnO_3$ system was studied. In this system the tolerance factors are close to 1, and because the ionic radii of La^{3+} and Pb^{2+} are close to each other the effect of A-site mismatch is minimal. Therefore, it was possible to study the effect of vacancies alone on the physical properties. The results show no appreciable effect of increasing vacancies on the lattice parameters; however, the effect of vacancies on the physical properties revealed that vacancies do change the variance factor σ^2. The concomitant disorder affects the magnetic and electrical properties by creating a distribution of Mn–O–Mn angles and Mn–O distances within the structure. However, clear ferromagnetic transition broadenings were not observed, which indicate that the long range order in manganese perovskite is determined by Mn–O–Mn angles that most deviate from 180° and Mn–O distances that are longest within the structure.

Acknowledgments

The authors are grateful to Dr. W.H. McCarroll for help with ICP analysis and to Dr. M. Lobanov for fruitful discussions. The NSF, Solid State Chemistry Grant DMR-99-07963, supported this work.

References

[1] L.M. Rodriguez-Martinez, J.P. Attfield, Phys. Rev. B 54 (1996) R15622.
[2] J.P. Attfield, Chem. Mater. 10 (1998) 3239.
[3] R.D. Shannon, Acta Crystallogr. A 32 (1976) 752.
[4] G. Popov, S.V. Kalinin, T. Alvarez, T.J. Emge, M. Greenblatt, D.A. Bonnell, Phys. Rev. B 65 (2002) 064426.
[5] W. Boujelben, A. Cheikh-Rouhou, J.C. Joubert, J. Solid State Chem. 156 (2001) 68.
[6] W.H. McCarroll, K.V. Ramanujachary, M. Greenblatt, F. Cosandey, J. Solid State Chem. 136 (1998) 322.
[7] G.H. Jonker, J.H. Van Santen, Physica 16 (1950) 337.
[8] S. Sundar Manoharan, N.Y. Vasanthacharya, M.S. Hegde, K.M. Satyalakshmi, V. Prasad, S.V. Subramanyam, J. Appl. Phys. 76 (1994) 3923.
[9] R. Mahendiran, R. Manesh, A.K. Raychaudhuri, C.N.R. Rao, J. Phys. D 28 (1995) 1743.
[10] M. Pechini, Method of preparing lead and alkaline-earth titanates and niobates, US Patent 3,330,697, 11 July 1967.
[11] DIFFRAC^{plus} TOPAS, User's Manual, Bruker AXS GmbH, Karlsruhe, Germany.
[12] H.Y. Hwang, S.-W. Cheong, N.P. Ong, B. Batlogg, Phys. Rev. Lett. 77 (1996) 1241.